Performance Test of CW 300 GHz Gyrotron FU CW I

Performance Test of CW 300 GHz Gyrotron FU CW I

T. Saito · T. Nakano · H. Hoshizuki · K. Sakai · Y. Tatematsu · S. Mitsudo · I. Ogawa · T. Idehara · V. E. Zapevalov

Abstract A 300 GHz CW gyrotron FU CW I has been developed and installed in the Research Center for Development of Far-Infrared Region, University of Fukui as a power source of a high frequency material processing system. Its performance was tested and the maximum power of 1.75 kW / CW has been attained at the beam voltage of 15 kV and the beam current of 1A. The maximum window power efficiency of 15.5% has been obtained at the cathode voltage slightly lower than 15 kV. This gyrotron is designed to deliver a Gaussian beam after mode conversion from the oscillation mode $TE_{22,8}$ in the cavity with a complex of an internal radiator and beam shaping mirrors. The detailed measurement with an infrared camera has confirmed that a Gaussian beam is radiated when the magnetic field strength B_c at the cavity is adjusted at a proper value. However, within a range of B_c, the output power is emerged into multiple directions, which suggests simultaneous oscillation of competing cavity modes.

Keywords FU CW I · Radiation pattern · Multi-mode oscillation

1 Introduction

Medium power millimeter / submillimeter waves have a very wide field of application. Among those promising applications are ceramic sintering and material processing. Magnetrons of 2.45 GHz are now most widely used. Recently, since a strong non thermal effect is expected for higher frequency power, use of 20–30 GHz gyrotrons is becoming popular [1, 2]. However, CW gyrotron with a further higher frequency has not been realized as a power source for practical applications including material processing, while a stronger non thermal effect and good focusing property due to a short wavelength can be expected.

T. Saito (✉) · T. Nakano · H. Hoshizuki · K. Sakai · Y. Tatematsu · S. Mitsudo · I. Ogawa · T. Idehara
Research Center for Development of Far Infrared Region, University of Fukui, Bunkyo 3-9-1,
Fukui 910-8507, Japan
e-mail: saitot@fir.fukui-u.ac.jp

V. E. Zapevalov
Institute of Applied Physics, RAS,
GYCOM Ltd., Nizhny Novgorod, Russia

The study of gyrotrons has a long history and there have since been two directions in gyrotron development [3]. One direction has been focused on high power gyrotrons. MW class gyrotrons are now being realized and applied to the thermonuclear fusion study represented by ITER. The other direction has aimed at high frequency gyrotrons. The record of oscillation frequency has steadily extended to higher frequencies [4] and very recently oscillation at a frequency exceeding 1 THz has been realized [5]. However, practical application of high frequency gyrotrons has been limited, because the main concern of the development of high frequency gyrotrons has been the challenge to high frequency and the study of gyrotron physics. Nowadays, application of high power submillimeter / terahertz range gyrotrons is just starting. In fact, high frequency gyrotrons are expected in various fields such as ceramics sintering [6, 7], highly sensitive protein analysis by using DNP-NMR [8], condensed matter physics [9, 10], new medical technology [11, 12], *etc.* Therefore, development of practically usable cw gyrotrons is very important for future evolution of the fields of gyrotron application [13].

FIR-FU (Research Center for Development of Far-Infrared Region, University of Fukui) has started a project of development of CW gyrotrons, FU CW I, CW II and CW III in a terahertz range. FU CW II delivers 394.6 GHz radiation of tens of Watts [14]. It will be used as a power source of DNP-NMR for protein analysis. FU CW III aims at fully continuous oscillation at a frequency over 1 THz with tens of Watts [15]. High power terahertz technologies will be developed with CW III.

FU CW I is a completely cw 300 GHz gyrotron with kW order power [16, 17]. It was developed for application to a material processing system. This gyrotron can also be used to development of the medical processing technology or the condensed matter physics such as submillimeter ERS measurement. Although a cw gyrotron in the 300 GHz frequency range and kilowatt order power had been demonstrated [18], FU CW I is the first gyrotron with these parameters for practical applications. It is installed in a 12 T liquid helium free superconducting magnet and works at the fundamental electron cyclotron resonance. It can be operated at a rather low cathode voltage of 15 kV and it is designed to radiate a Gaussian beam. FU CW I is therefore suitable for practical applications.

Its performance test has been carried out in advance of the commissioning in the material processing system. The maximum cw output power of 1.75 kW has been attained. The radiation pattern was measured and radiation of a single Gaussian beam with a very low level of the side lobe was confirmed. However, the maximum power is lower than the design value of 3.5 kW. Moreover, mode competition was observed in a range of the parameter space of the magnetic field strength at the cavity and the cathode voltage. Several modes oscillated simultaneously. This resulted in radiation of the output power into multi directions. Then the radiation pattern was measured in detail by using an infrared camera to study the oscillation characteristics of this gyrotron. This measurement is very important to find the way to higher power. It also provides interesting physics of high frequency gyrotrons.

The outline of this paper is as follows. Section 2 describes the specifications of FU CW I. Section 3 provides the results of the performance test. The measurement of the radiation pattern is shown in Section 4 and discussion is made in Section 5 on the oscillation characteristics by using simple analyses. Finally, Section 6 is devoted to conclusions.

2 Specifications of FU CW I

The frequency of FU CW I is 300 GHz. The design value of the output power is 3.5 kW / CW for the cathode voltage of 16±1 kV and the beam current of 1.1±0.1 A. Design

optimization has been carried out on the base of computer simulation [16]. This gyrotron was manufactured by Gycom Ltd. The electron beam emitter is made of LaB_6. The cathode radius is 21.5 mm. Although the structure of the electron gun is of triode type, the anode potential is set at the cavity voltage. Thus this gyrotron operates as a diode tube. The designated cavity mode is $TE_{22,8}$. The radius of the flat region of the cavity R_c is 8.39 mm. The electron beam radius R_b in the cavity is set to be 3.71 mm corresponding to the first maximum of the coupling coefficient between the electron beam and the wave electric field. The resonance frequency of the $TE_{22,8}$ mode is almost 300 GHz but slightly less than 300 GHz. The length of the flat region of the cavity is 15 mm and the total Q value including the Ohmic loss is about 6000. Owing to a relatively large cavity radius with a higher mode such as $TE_{22,8}$, the Ohmic loss in the cavity is suppressed to less than 0.3 kW/cm^2. FU CW I is installed in a liquid helium free 12 T super conducting magnet of which the diameter of the room temperature bore is 100 mm. The outer diameter of the cavity section inserted into the bore is 90 mm. Oscillation is at the fundamental electron cyclotron frequency. Auxiliary ordinary conducting coils are installed at the electron gun position. They are used to adjust the electron beam radius in the cavity.

A mode converter composed of a radiator of Vlasov type and three beam shaping mirrors is equipped inside the gyrotron. The output power shaped in a Gaussian beam is reflected off an additional plane mirror and delivered through the vacuum window into the horizontal direction. The final mirror can be tilted to adjust the output beam direction. The vacuum window is made of boron nitride. Its diameter is 80 mm. In advance of the detailed measurement of the radiation pattern, the angle of the final mirror was adjusted for the main $TE_{22,8}$ mode to be radiated to the direction normal to the plane of the flange of the vacuum window. This was carried out observing the radiation patter with an infrared camera. The spent electron beam is absorbed on the surface of the collector located in the upper part of the gyrotron. The outer diameter of the collector section is 137 mm. The internal structure and the outer shape of FU CW I is similar to high power gyrotrons that are used for electron heating in magnetic fusion devices. This gyrotron can be operated either in CW mode or in pulse mode.

When it is used as the power source of the material processing system [6, 7], the output power is coupled to an applicator through a corrugated waveguide with the inner diameter of 63.5 mm [6]. Uniform power distribution is expected in the applicator owing to the small wavelength compared to the diameter of the applicator of 500 mm. Spot heating mode is also available by setting a focusing mirror in front of the open end of the corrugated waveguide. The spot size of the order of millimeter is possible and the power density becomes a level of MW/m^2.

3 Oscillation TEST of FU CW I

The output power P_{out} was measured with a water load. The water load was set just out side of the vacuum window. The dependence of the output power P_{out} on the magnetic field strength B_c at the cavity was first measured. Figure 1 plots P_{out} in the region of B_c in which the $TE_{22,8}$ mode is excited. The coil current of the 12 T magnet can be adjusted with a step of 0.1 A corresponding to about 7.5×10^{-3} T. The cathode voltage V_c was 12.5 kV. The measurement of the radiation pattern described in the next section shows that, at this voltage, the output beam is radiated to one direction within a rather wide range of B_c. The beam shape has an almost Gaussian cross section. The peak value of P_{out} was obtained around B_c of 10.91 T and decreased to about half value of the peak power for the variation of about 0.03 T, which will be discussed in the next section.

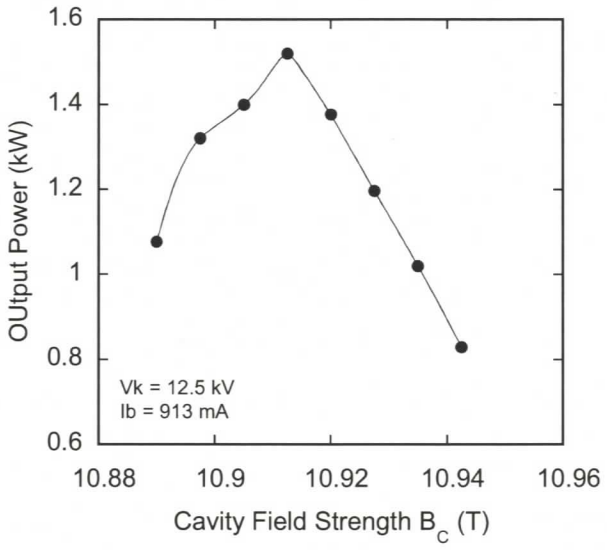

Fig. 1 Dependence of the output power on the cavity field. The cathode voltage is 12.5 kV.

Then, the cathode voltage dependence of P_{out} was tested with B_c being fixed at 10.91 T. The beam current I_b was 0.91 A. Figure 2 depicts the measured result. Oscillation starts at V_C slightly less than 8 kV and P_{out} increases with V_c to a maximum power at 12.5 kV. However, P_{out} saturates for larger V_c. The dependence of P_{out} on V_C shows a hysteresis phenomenon. Figure 2 shows a cycle of V_c variation and P_{out} measured in the phase of upward variation of V_c is somewhat different than P_{out} measured in the downward variation phase. The most clear difference is seen at V_c around 10 kV. The measured data has three peaks as indicated by arrows in Fig. 2. This implies a possibility of mode transition depending on V_c. The cathode voltage at which P_{out} becomes maximum slightly increases with B_c within the range shown in Fig. 1. This may be explained by the increase in the relativistic factor with B_c. The highest efficiency as defined as the ratio of the water load power measured at just outside of the vacuum window to the electron beam power is 15.5%.

Next, dependence of P_{out} on I_b was measured. This measurement was done aiming at higher power and the maximum rating of V_c and I_b was set. Figure 3 plots the output power

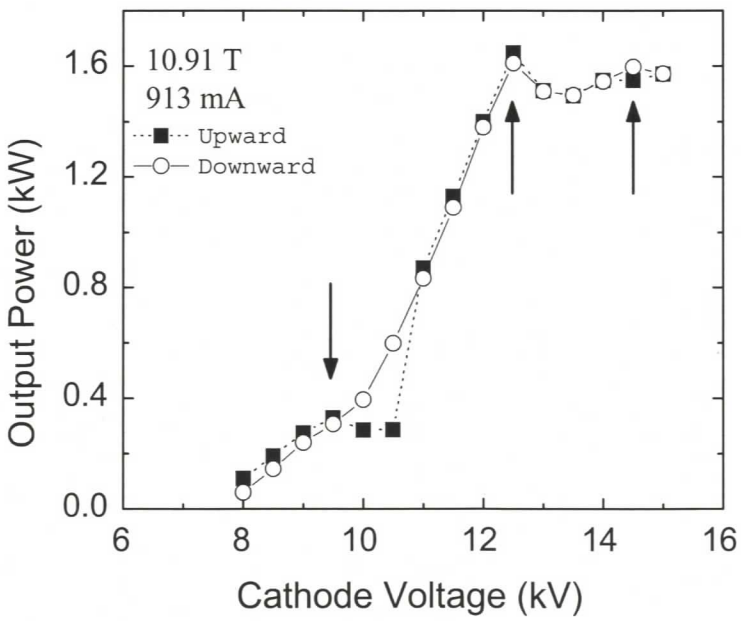

Fig. 2 Output power measured with a water load as a function of the beam voltage.

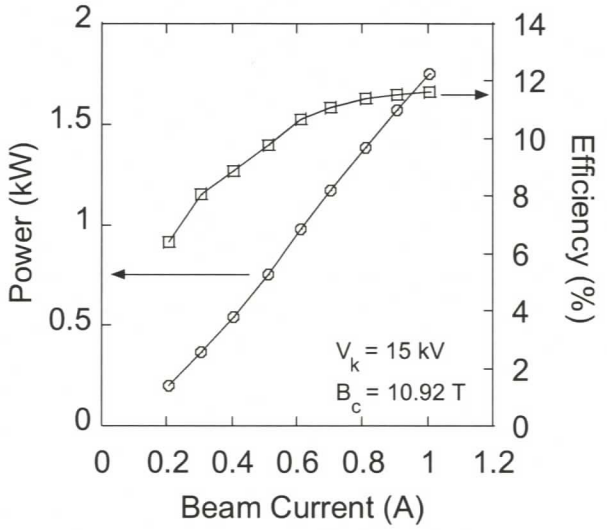

Fig. 3 Output power and the window efficiency are plotted as functions of eh electron beam current.

P_{out} as a function of I_b. The cathode voltage and the cavity field were fixed at 15 kV and 10.92 T, respectively. The value of P_{out} increases almost linearly with I_b up to 1 A, the maximum rating of I_b. The maximum value of P_{out} reached 1.75 kW at 1.0 A. The efficiency was 11.5% for P_{out} of 1.75 kW. Therefore, P_{out} has not attained at the nominal power of 3.5 kW yet and the heating power available to material processing is limited at the moment. Two water loads of different types were utilized in the power measurement. One is a Teflon tube type and the other is a SiC type. The measured output power with the two water loads agreed within 5 % for the same operation condition.

The oscillation frequency f was measured to identify the oscillation mode. A small part of the output power was guided to a harmonic mixer and mixed with a highly stabilized local oscillator power with f_{LO}. The intermediate frequency f_{IF} output from the mixer was fed into a spectrum analyzer. Then the oscillation frequency determined as the sum of or difference between nf_{LO} and f_{IF}, where n is the harmonic number. In this measurement V_c was varied and B_c was fixed at the value for which the maximum power was obtained for V_c of 12.5 kV. Step like changes of the measured frequency was observed as shown in Table 1. This suggests that three oscillation modes oscillate depending on V_c, which is consistent with the power measurement shown in Fig. 2.

For a range of low value of V_c, the measured frequency is 300.4 GHz that is slightly larger than the resonance frequency of the $TE_{22,8}$ mode. In the middle range of V_c including the condition of Fig. 1, the measured frequency is 299.2 GHz. This frequency is very close to the resonance frequency 299.6 GHz of the $TE_{22,8}$ mode. Therefore, the oscillation mode corresponding to this frequency is identified as the $TE_{22,8}$ mode. The measured frequency is slightly less than the resonance frequency. A fabrication error of the cavity radius is a possible candidate. The relative frequency difference is about $0.4/300 \approx 1.3 \times 10^{-3}$. If the cavity radius is larger than 8.39 mm by about 10 μm, this frequency difference can be

Table 1 Observed frequency in each voltage span.

V_c (kV)	f (GHz)
8–9	300.4
10–12.5	299.2
13–15	297.6, 299.2

explained. Further increase in V_c brings about oscillation of another mode. This mode has a frequency of 297.6 GHz. This frequency is close to the resonance frequency 297.4 GHz of $TE_{19,9}$ mode. The counter rotating $TE_{19,9}$ mode is the most dangerous competitive mode because the radius of the electron beam at which the coupling coefficient has the first maximum is very close to that of the $TE_{22,8}$ mode. Therefore, we consider that the new mode is the $TE_{19,9}$ mode. Mode identification is discussed in more detail in Section 5.

4 Measurement of radiation pattern

Measurement of the radiation pattern has several meanings. Confirmation that the output beam is radiated as a Gaussian beam is the first necessity. Secondly, beam parameters such as the diameter and the position of the beam waist of the Gaussian beam are necessary for effective power transmission to the applicator. Thirdly, this measurement provides insight into the oscillation modes in the cavity.

A plate of polyvinyl chloride (PC) 1 mm in thickness was placed normal to the output beam at some distance from the vacuum window as a power absorber. The distribution of the temperature increase of the plate was recorded with an infrared camera from the reverse side to the gyrotron. This measurement was carried out in a pulse mode to avoid burning of the absorber plate. The duty factor was 5 %. A simple analysis of thermal diffusion with the material constants of the PC plate shows that the diffusion length is about 1 mm during 10 s. Thus, we can consider that the measured temperature profile well reflects the power profile as long as measurement is carried out within a few tens of seconds.

Figure 4 shows an example of the measured radiation pattern. It can be seen that the radiated beam has a power profile peaked on the center of the cross section but slightly elongated vertically. Temperature profiles along the horizontal and vertical lines passing the temperature peak are plotted in Figs. 5 (a) and (b). The dashed lines stand for the best fit Gaussian profiles. The temperature profiles along both directions are well fitted to Gaussian curves. However, cross section has an prolate shape along the vertical direction. An e-folding radius w_E of the wave electric field is derived as $\sqrt{2}$ times that of the temperature distribution w_T as long as the temperature profile stands for the power density profile. The present measurement is the case.

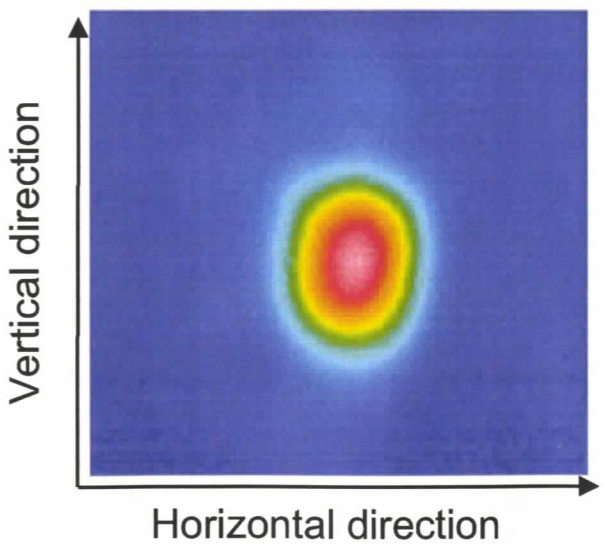

Fig. 4 An infrared camera Image of the radiation pattern.

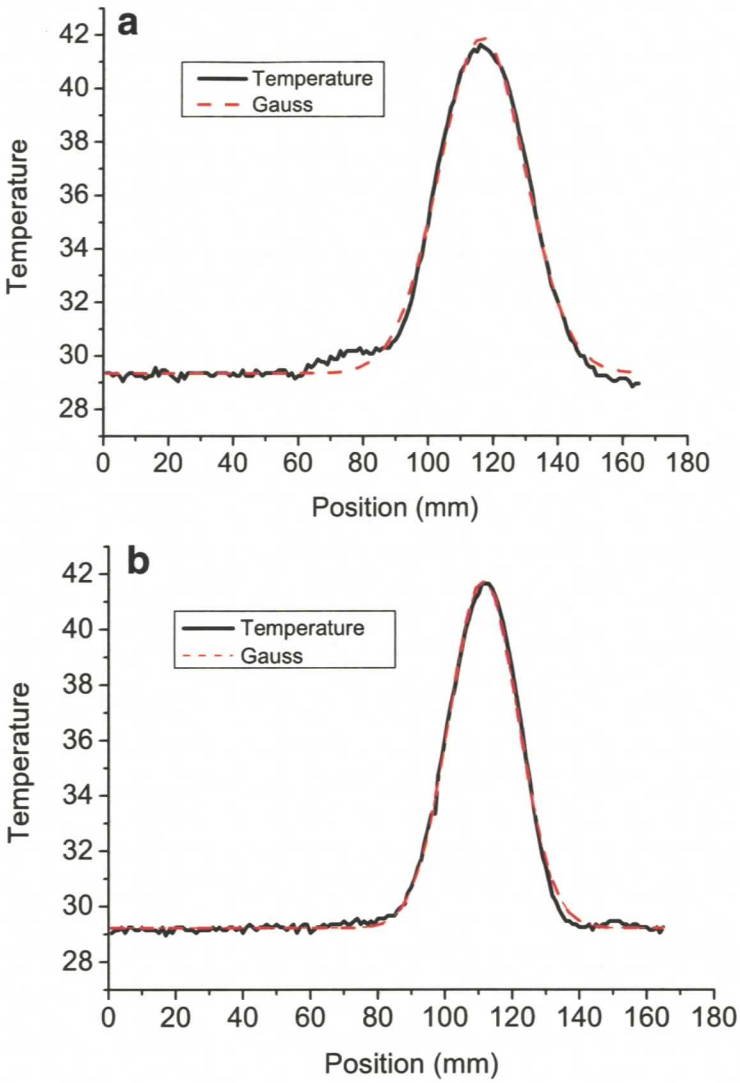

Fig. 5 Temperature distribution along (a) the vertical and (b) the horizontal lines passing the peak temperature point.

The same measurement was carried out at different distances from the vacuum window. Figure 6 plots w_E for the horizontal and vertical directions as functions of the distance z from the flange of the vacuum window. The e-folding radii increase with z. The solid lines represent fitting curves for a bi-Gaussian beam.

$$w_{E\alpha}^2(z) = w_{0\alpha}^2 \left\{ 1 + \left[\frac{\lambda(z - z_{c\alpha})}{\pi w_{0\alpha}^2} \right]^2 \right\}.$$

Here, w_0 is the spot size at the beam waist and z_c stands for the position of the beam waist measured from the flange of the vacuum window. The suffix α indicates horizontal or vertical direction. The data points closely lie on the fitting curves, with horizontal w_0=1.4 cm and vertical w_0=1.5 cm. These values are almost equal within the experimental accuracy. The output beam is confirmed to be a Gaussian beam but it is slightly elongated along the vertical direction. This elongation comes from the difference between the positions of the beam waists for the horizontal and vertical directions. The radiation pattern just outside of the vacuum window includes a low level of side lobes.

The above measurement has shown that FU CW I radiates a single Gaussian beam in a properly adjusted operation parameter range. However, a multi peak character of the radiation pattern reveals in the range of V_c corresponding to multi frequency oscillation

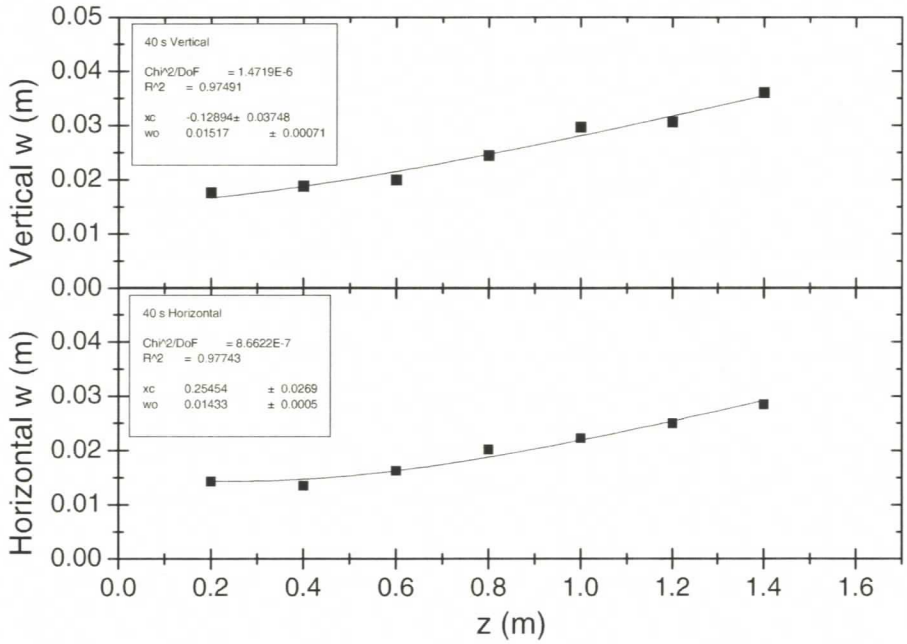

Fig. 6 E-folding radii of the field amplitude are plotted as functions of the distance from the flange of the vacuum window.

described in the previous section [19, 20]. Figure 7 represents an IR camera image of the temperature profile for a case of two peaks. The cathode voltage V_c was 15 kV. The multi peak radiation pattern sensitively depends on B_c and V_c. For $V_c \leq 12$ kV, a single peak radiation is observed within almost all range of B_c. This is the same situation as that of only $TE_{22,8}$ mode oscillation was observed in the frequency measurement.

Figure 8 shows the temperature distribution of the absorber along the horizontal direction for different B_c. Multi peaks always appear along the horizontal direction and the position corresponding to each peak is fixed. Therefore, each peak is considered to correspond to different oscillation mode. As shown by the solid line in Fig. 8, only one beam is radiated in the condition when B_c is set at 10.95 T. This beam is radiated to the same direction as that for V_c of 12 kV. At this cathode voltage only one beam is radiated and the direction does not change for different value of B_c within the range of Fig. 3. This

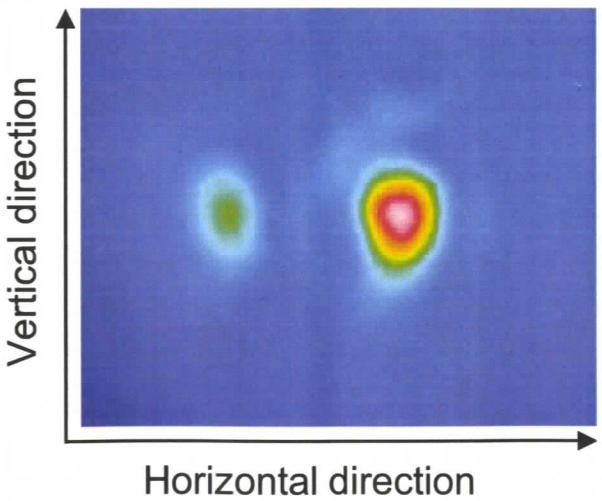

Fig. 7 An example of IR camera image of the temperature profile for a case of two peaks.

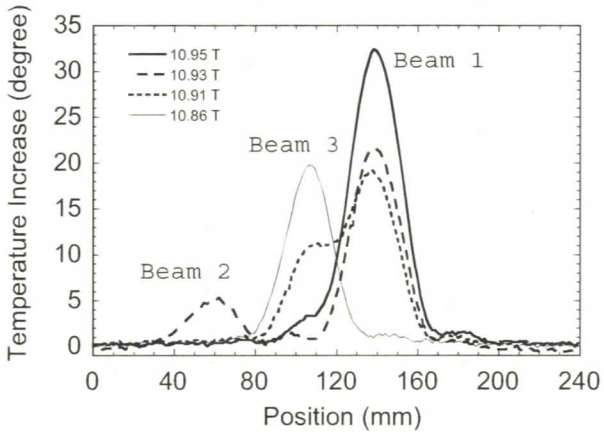

Fig. 8 Variation of the radiation pattern with the magnetic field strength in the cavity.

oscillation was identified to be the $TE_{22,8}$ mode from the frequency measurement. Thus, it can be concluded that the radiation shown by the solid line in Fig. 8 originates from the $TE_{22,8}$ mode. We refer to this beam as Beam 1.

The peak temperature of the absorber corresponding to the power of Beam 1 decreased with decreasing B_c. A new peak appeared in the position left to the peak of Beam 1 when B_c was slightly decreased as depicted by the dashed line in Fig. 8. We call this beam as Beam 2. The output power of the oscillation corresponding to this peak was rather low and disappeared for smaller B_c. Instead, another peak turned up in between Beam 1 and Beam 2. The dotted line in Fig. 8 stands for this case. This peak is referred as Beam 3. When B_c is further decreased, Beam 1 disappeared and Beam 3 alone was observed as shown by the thin solid line in Fig. 8. The difference of B_c between the case of the solid line and the case of dotted line is 0.09 T. We will discuss this in the next section.

Figure 9 plots the peak temperatures corresponding to each beam as functions of B_c. The cathode voltage was fixed at 15 kV. The peak temperatures can be used as a relative measure of the power variation in each mode. For comparison between different beams, integration of the temperature increase in the cross section of each beam is necessary and power transmission efficiency of the mode converter should be considered for each beam. Beam 1 was identified as $TE_{22,8}$ mode. The oscillation power of this mode attains to maximum at B_c of about 10.97 T and decreases with decreasing B_c. Oscillation of this mode stops at B_c between 10.87 T and 10.88 T. Beam 2 represented by the closed circle in Fig. 9

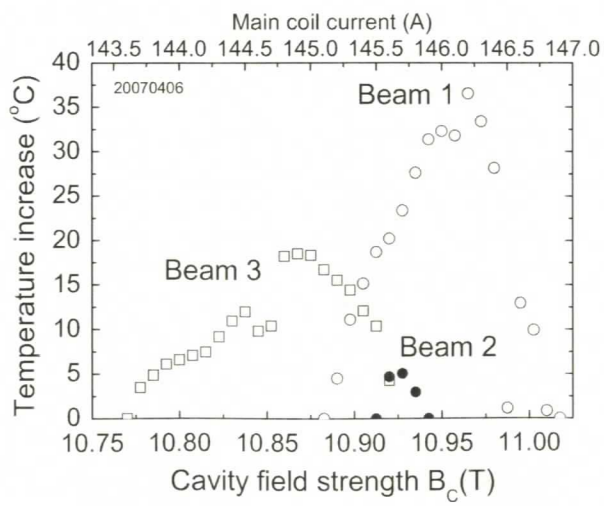

Fig. 9 Temperatures at the peaks of Beam1, 2 and 3 are plotted as functions of B_c for the case of V_c of 15 kV.

appears in a narrow range of B_c and the output power is rather small. The oscillation mode corresponding to Beam 2 has not been definitely identified yet. Candidates of this mode will be listed in the next section. With further decreasing B_c, Beam 3 comes in instead of Beam 2 and its power increases with decreasing B_c. It predominates for B_c smaller than 10.90 T and finally single mode oscillation takes place. The output power of this mode becomes maximum at B_c of about 10.87 T. Although it is inferred that Beam 3 originates from $TE_{19,9}$ mode, further discussion will be given in the next section.

The radiation pattern has been measured in the pulse mode but the infrared camera records the temperature profile of the absorber plate as a result of time integration of the absorbed power. Therefore, the multi peak pattern does not directly means simultaneous oscillation of multi modes. Then, pyroelectric detectors were set on the lines of Beam 1 and 3. The measured wave form from the two detectors clearly showed that the two modes corresponding to each beam simultaneously oscillated during full width of the cathode voltage pulse. The dependence of the signal intensities on B_c was similar to the dependence as shown in Fig. 9.

As shown above, the oscillation mode changes depending of the combination of V_c and B_c. Therefore, "mode mapping" is important. Figure 10 shows this mapping for operation with I_b=1 A. The vertical lines represent the B_c ranges within which Beams 1 (solid line), 2 (thick solid line) and 3 (dashed line) were observed. Overlap of two lines indicates simultaneous oscillation of the corresponding beams. The area for Beam 1 corresponding to the $TE_{22,8}$ mode has a triangle shape. The right boundary of V_c is due to the operation limit of the gyrotron. The upper boundary of B_{cU} decreases with decreasing V_c maintaining the condition B_{cU}/γ = constant. Here, γ is the relativistic factor. On the other hand, the lower boundary does not vary significantly with V_c. The oscillation range in B_c disappears at V_c around 8.5 kV. The area of Beam 3 locates below the area of Beam 1. The right boundary of V_c is also due to the operation limit. Similarly to the case of Beam 1, the upper boundary of B_c decreases with decreasing V_c. The oscillation range in B_c does not disappear down to 6.5 kV. The power supply does not wok below this voltage and the real lower voltage boundary cannot be examined at the moment. Two areas overlap in a voltage range near 15 kV. Two modes simultaneously oscillate in the overlapping area. This corresponds to the power saturation range in Fig. 2. Single oscillation of the $TE_{22,8}$ mode is realized in the

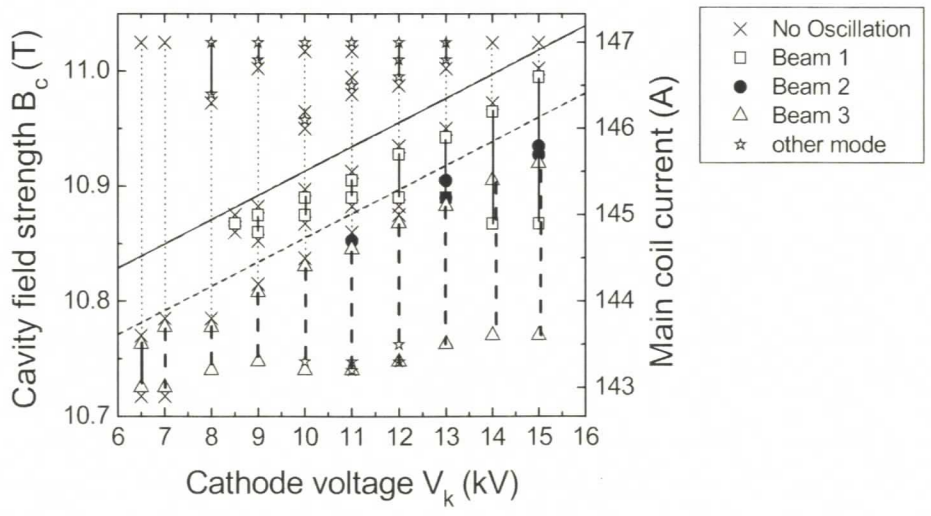

Fig. 10 Mapping of oscillation range of each mode.

non-overlapping area. Oscillation of the competing modes is seen in the smaller B_c region. The radiation power corresponding to Beam 2 is low and Beam 2 is observed only in a limited area.

The power measurement shown in Fig. 2 was done with B_c being fixed at 10.91 T. The measured oscillation frequency, as shown in Table 1, was 300.4 GHz in the region left to the $TE_{22,8}$ mode region. Candidate modes corresponding to 300.4 GHz oscillation will be cited in the next section. Moreover, a further new oscillation mode was seen in the up-left region of Fig. 11.

5 Discussion

The performance test of FU CW I and the measurement of the radiation pattern have provided valuable information in advance of application of FU CW I to material processing. However, important problems have been revealed. The first problem is the saturation of the output power against the cathode voltage. The second problem is that the output power is radiated into multi directions and simultaneous oscillation of competing modes occurs in a range of the operation condition. Two problems probably couple with each other. We briefly discuss these problems in this section. We also try to identify the oscillation modes observed in the measurement of radiation pattern.

We referred to the $TE_{19,9}$ mode as a prime candidate of the mode competing to the main mode $TE_{22,8}$. We begin with examination of this possibility. The condition for oscillation of a specific mode in a gyrotron is matching between the resonance frequency f_c of the mode in the cavity and the electron cyclotron harmonic frequency sf_{ce}. Here, s is the harmonic number. Although f_c is not exactly equal to sf_{ce} but slightly higher than sf_{ce} for gyrotron oscillation to take place, the oscillation mode is predominantly determined by this condition. However, because the cavity radius R_c is much larger than the wavelength in a high frequency gyrotron or a high power gyrotron, the mode density is very high and many modes become possible to oscillate at the same cavity field strength B_c. Then, as the second condition of mode selection, the radius R_b of the electron beam injected into the cavity in a cylindrical shape should be carefully adjusted for the designated mode to overcome competing modes. This condition is expressed with the coupling coefficient between the

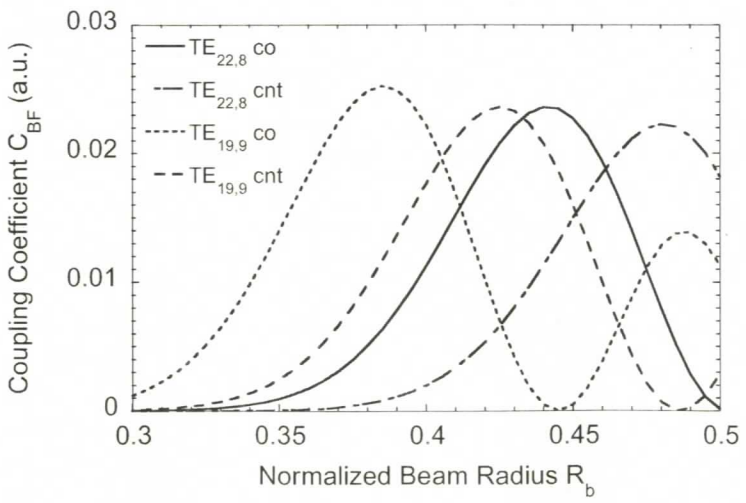

Fig. 11 Coupling coefficients of the four modes are plotted as functions of the normalized radius of the electron beam in the cavity.

electron beam and the wave electric field. The coupling coefficient C_{BF} of $\mathrm{TE_{mp}}$ mode is given by [21].

$$C_{BF} = \frac{\chi_{mp}^2 J_{m\pm s}^2(k_{mp}R_b)}{\pi R_c^2\left(\chi_{mp}^2 - m^2\right)J_m^2(\chi_{mp})},$$

where $J_{\mathrm{m-s}}$ and $J_{\mathrm{m+s}}$ are taken for the co-rotating mode and counter-rotating mode, respectively. The cut off wave number is given by $k_{mp} = \chi_{mp}/R_c$ with the p-th zero χ_{mp} of the derivative of the m-th Bessel function of the first kind. The beam radius is usually set at $R_b = R_c\,\chi_{m\pm s,1}/\chi_{mp}$ at which C_{BF} has the first maximum. The design value R_b=3.71 mm corresponds to this condition for the co-rotating $\mathrm{TE_{22,8}}$ mode.

Oscillation of a competing mode cannot be fully excluded even with these careful adjustments. Figure 11 plots C_{BF} for the $\mathrm{TE_{22,8}}$ mode and the $\mathrm{TE_{19,9}}$ mode as functions of the normalized injection radius $r=R_b/R_c$ of the electron beam. The coupling coefficient of the co-rotating $\mathrm{TE_{22,8}}$ mode has a maximum value at r=0.442, while that of the counter-rotating $\mathrm{TE_{19,9}}$ mode has a maximum value at r=0.425 and the maximum of C_{BF} of the co-rotating $\mathrm{TE_{19,9}}$ mode is located at r=0.385. There is certainly a high possibility of oscillation of the counter-rotating $\mathrm{TE_{19,9}}$ mode. Moreover, the co-rotating $\mathrm{TE_{19,9}}$ mode also has a chance of oscillation if the electron beam is injected at smaller radius less than 0.40. There are similar competition between the designated mode and a spurious mode, such as between co-rotating $\mathrm{TE_{22,6}}$ mode and counter-rotating $\mathrm{TE_{19,7}}$ mode [22], between co-rotating $\mathrm{TE_{28,7}}$ mode and counter-rotating $\mathrm{TE_{25,8}}$ mode [23], and between co-rotating $\mathrm{TE_{31,8}}$ mode and counter-rotating $\mathrm{TE_{28,9}}$ mode [24].

Next we consider the cathode voltage dependence of the output power as depicted in Fig. 2. In this measurement, the cavity field B_c was fixed at 10.91 T that was optimum for V_c=12 kV. However, an increase in V_c is equivalent to a decrease in B_c. The increment by 3 kV in V_c from 12 kV to 15 kV results in an increase in the relativistic factor by the ratio of 1.006 and causes an equivalent decrease of B_c by the same ratio. This ratio is almost equal to 1.007 as the ratio of the resonance frequency of $\mathrm{TE_{22,8}}$ mode to that of the $\mathrm{TE_{19,9}}$ mode. Thus this variation of V_c under fixed B_c could lead to oscillation of $\mathrm{TE_{19,9}}$ mode.

We examine this possibility from an analytic calculation of the starting current I_{s}. An analytic expression of the starting current is given in Refs. [21, 25].

$$\frac{-1}{I_s} = \frac{QZ_0e}{8\gamma_0 m_e c^2}\left(\frac{\pi}{\lambda}\int_0^L \left|\widehat{f}(z)\right|^2 dz\right)^{-1} \frac{C_{BF}}{(\beta_{z0}(s-1)!)^2}\left(\frac{ck_{mp}\gamma_0\beta_{\perp 0}}{2\Omega_0}\right)^{2(s-1)}$$

$$\times\left(s + \frac{1}{2}\frac{\omega\beta_{\perp 0}{}^2}{v_{z0}}\frac{\partial}{\partial\Delta_s}\right)\left|\int_0^L \widehat{f}(z)e^{i\Delta_s z}dz\right|^2,$$

where, Z_0 is the wave impedance in free space, $\widehat{f}(z)$ is the normalized axial distribution of the wave electric field in the cavity and $\Delta_s = (\omega - s\Omega_0/\gamma_0)/v_{z0}$ is the frequency mismatch parameter. The diffractive Q value is approximated to be

$$Q_D = 4\pi\left(\frac{L}{\lambda}\right)^2 \frac{1}{1 - R_{out}}$$

with the reflection coefficient R_{out} at the output end of the cavity [26]. The total Q includes the Ohmic Q value [21]. Other symbols are used in a usual manner. The starting current can be calculated with an acceptable assumption that $\widehat{f}(z)$ has a Gaussian profile.

Figure 12 plots I_s of the $TE_{22,8}$ mode and the $TE_{19,9}$ mode as functions of B_c for two values of V_c. The normalized injection radius R_b is set to be 0.44. This is the nearly optimum value for the $TE_{22,8}$ mode. The pitch factor is 1.4. This is the design value. The $TE_{22,8}$ mode has a minimum starting current for V_c=12 kV at the fixed B_c=10.93 T. The oscillation region of the $TE_{22,8}$ mode moves to right, i.e. a higher B_c region with V_c. The oscillation region of the $TE_{19,9}$ mode initially located in the left region for 12 kV also moves to right with V_c. Then, as expected from the qualitative estimation given above, the starting current of the $TE_{19,9}$ mode becomes comparable to that of the $TE_{22,8}$ mode for V_c=15 kV at B_c=10.93 T. Therefore, in principle, oscillation of the $TE_{19,9}$ mode can take place when V_c is increased and consequently saturation of the output power may result. In addition, the difference between the upper bounday of B_c of the $TE_{28,8}$ mode and that of the $TE_{19,9}$ mode at the same V_c is about 0.08 T. This is nearly equal to the difference of the upper boundaries of the areas of Beam 1 and 3 in Fig. 10. This also supports that Beam 3 originates from the $TE_{19,9}$ mode.

For lower beam current operation, say, I_b=0.6 A, the upper boundaries of B_c the oscillation area of the two modes as shown in Fig. 11 do not change significantly but the

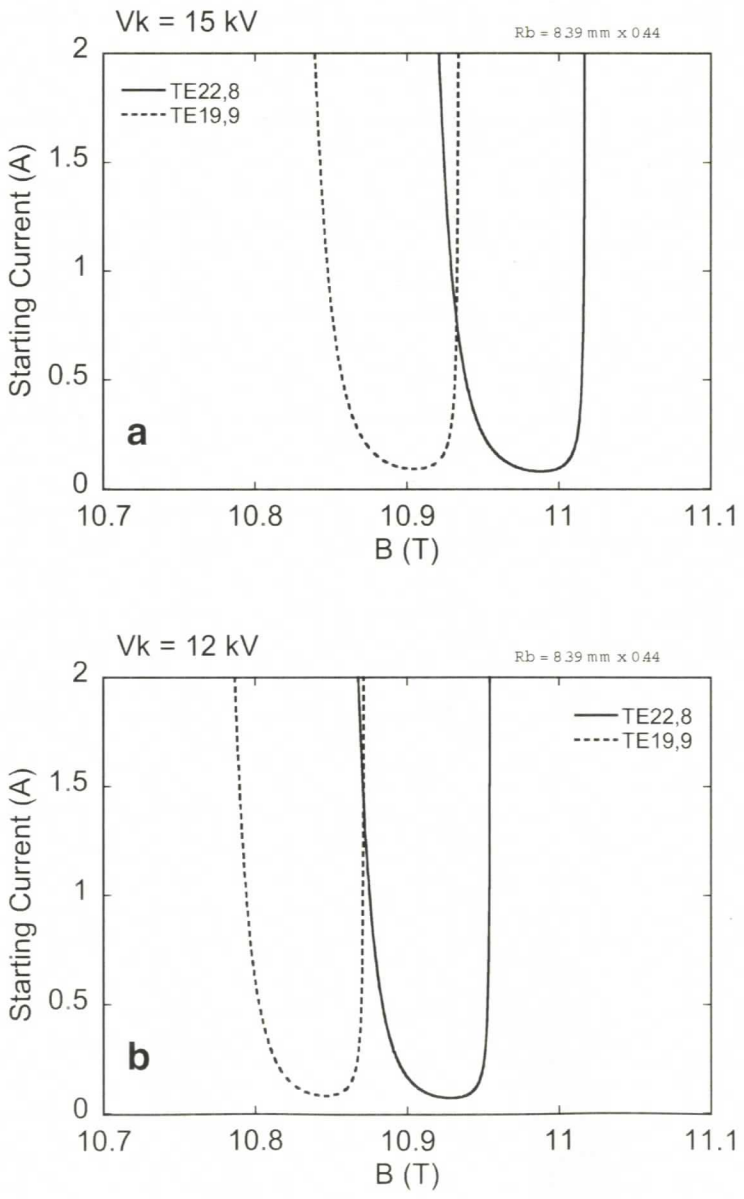

Fig. 12 Starting currents for two modes are plotted as functions of the cavity field B_c. (**a**) V_k=15 kV; (**b**) V_k=12 kV. The normalized injection radius is 0.44 and the pitch factor is 1.4.

lower boundaries somewhat increases. As plotted in Fig. 12 (a), I_s sharply increases on the high B_c side but rather gradually increases with decreasing B_c on the low field side. Then, the upper boundary of B_c does not change with I_b but the lower boundary of B_c increases with decreasing I_b. When I_b was decreased to 0.3 A, the B_c region of simultaneous oscillation of the two modes disappeared.

Some important problems remain open. One is theoretical understanding of simultaneous oscillation of the competing modes. Experimentally, we have observed simultaneous oscillation of two modes. The simple analysis presented above has also shown overlapping of the oscillation region of the two modes. Figure 12 (a) indicates overlapping of the B_c region in which I_s is smaller than 1.0 A for Vk=15 kV. On the other hand, as shown in Fig. 12 (b), the overlapping region disappears for Vk=12 kV. This corresponds to the experimental observation that simultaneous oscillation did not take place at 12 kV. However, overlapping of the B_c region does not directly mean simultaneous oscillation. It is difficult to point out the physical mechanism of the simultaneous oscillation at the moment. Non linear mode interaction through electron beam modulation had been pointed out as a possible cause of multi mode oscillation [27]. It is also likely that misalignment such as off-axis injection or inclination of the electron beam axis to the cavity axis enhances mode competition and simultaneous oscillation of two modes. For further discussion, more detailed study relying on proper numerical simulation is necessary. This is beyond the scope of this paper and detailed theoretical analysis will be presented elsewhere.

The other problem is the rotation direction of the $TE_{19,9}$ mode. We have identified the Beam 3 as the $TE_{19,9}$ mode without specification of the rotating direction. Counter-rotating $TE_{19,9}$ mode competes with the co-rotating $TE_{28,8}$ mode. However, counter-rotating mode power is not efficiently radiated form the Vlasov radiator designed for co-rotating modes. The electron beam radius has a large effect for discrimination of the rotating direction. In fact, if the normalized injection radius R_b is less than 0.40, the co-rotating $TE_{19,9}$ mode has lower starting current than that of the counter-rotating $TE_{19,9}$ mode. Decision of the rotating direction is also the next task.

In Fig. 2, one mode can be seen for V_c less than 10 kV. The measured frequency of this mode is 300.4 GHz. Candidate cavity modes with the similar frequencies are $TE_{12,12}$, $TE_{25,7}$, $TE_{28,6}$. The normalized beam radiuses corresponding to the first maximum of the coupling coefficient of co-rotating modes are 0.243, 0.499, 0.557, respectively. Among three modes, the $TE_{25,7}$ mode has a starting current less than 0.3 A at B_c of 10.91 T through 10.92 T. The starting current of the other two modes is much larger than 1.0 A at same B_c. Thus, the $TE_{25,7}$ mode is most probable as the 300.4 GHz mode but further discussion is difficult from the present observation only.

Moreover, the oscillation mode corresponding to Beam 2 is also unknown. Several cavity modes exist between the $TE_{19,9}$ mode and the $TE_{22,8}$ mode. Based on a simple calculation of the starting current, $TE_{3,16}$ mode and then $TE_{5,15}$ mode may become a predominant mode within a narrow range of B_c between the $TE_{22,8}$ dominant and $TE_{19,9}$ dominant regions. Recently a numerical simulation including nonlinear interaction between oscillation modes has suggested the $TE_{3,16}$ mode is more likely as the mode corresponding to Beam 2 [28]. However, the oscillation frequency corresponding to these modes has not been identified yet. Therefore, mode identification corresponding to Beam 2 remains open.

6 Conclusions

A 300 GHz cw gyrotron FU CW I has been developed and installed in Research Center for Development of Far-Infrared Region, University of Fukui. Its performance was tested in

advance of application to the material processing system. Stable cw operation with the designated $TE_{22,8}$ mode was confirmed. The maximum efficiency of the window power was 15.5%. The maximum window power has attained to 1.75 kW. Radiation of the output power in a Gaussian beam was confirmed. This shows that the internal mode converter woks well. The performance test has shown that FU CW I can be used as a power source of the material processing system.

However, the output power saturated with the beam voltage. Frequency measurement has shown mode transition with the cathode voltage and simultaneous oscillation of a parasitic mode. Then, radiation pattern of FU CW I was measured in detail with an infrared camera and rather complicated oscillation characteristics has emerged. Single mode oscillation of the design mode was realized only in a particular range in the B_c–V_c space. Radiation into multiple beams took place out side of this region. Mode transition phenomenon was also observed when B_c was decreased with a fixed V_c. Simultaneous oscillation of competing modes corresponding to each of the multiple beams was confirmed by using pyroelectric detectors with a enough time resolution.

Possibility of mode competition and /or mode transition was suggested from simple analyses with the coupling coefficient and the starting current. More detailed theoretical analysis is the next task.

FU CW I will be soon under commissioning for ceramic sintering experiment. The short wavelength of 1 mm of radiation from FU CW I leads to good focusing property and the effect of high power density can be expected. The short wavelength also provides a possibility of development of a new medical processing technology. Moreover, it is possible to use FU CW I as a power source of high frequency ESR experiment.

References

1. Y. V. Bykov, K. I. Rybakov, and V. E. Semenov, J. Phys. D: Appl. Phys. **34**, R55 (2001)
2. H. Hoshizuki, S. Mitsudo, T. Saji, K. Matsuura, T. Idehara, M. Glyavin, *et al.*, Int. J. Infrared Millim. Waves **26**, 1531 (2005)
3. See references cited in M. Thumn, "State-of-the-Art of High Power Gyro-Devices and Free Electron Masers Update 2005", FZKA 7198, 2006.
4. T. Idehara, I. Ogawa, S. Mitsudo, M. Pereyaslavets, N. Nishida, and K. Yoshida, IEEE Trans. Plasma Sci. **27**, 340 (1999)
5. T. Idehara, H. Tsuchiya, O. Watanabe, La Agusu, and S. Mitsudo, Int. J. Infrared Millim. Waves **27**(3) (2006) DOI 10.1007/s10762-006-9084-9.
6. H. Hoshizuki, K. Matsuura, S. Mitsudo, T. Idehara, O. V. Malygin *et al.*, Conf. Digest of 30th IRMMW & 12th THz (2005) 375.
7. S. Mitsudo, K. Sakai, T. Idehara, *et al.*, Conf. Digest of 31th IRMMW & 14th THz (2006) p.572.
8. V. Bajaj, C. Farrer, M. Hornstein, I. Mastovsky, J. Vieregg, J. Bryant, B. Elena, K. Kreischer, R. Temkin, and R. Griffin, J. Mag. Res. **160**, 85 (2002)
9. T. Tatsukawa, T. Maeda, H. Sasai, T. Idehara, M. Mekata, T. Saito, and T. Kanemaki, Int. J. Infrared Millim. Waves **16**, 293 (1995)
10. S. Mitsudo, T. Aripin, T. Shirai, T. Matsuda, T. Kanemaki, and T. Idehara, Int. J. Infrared Millim. Waves **21**, 661 (2000)
11. T. Tasukawa, A. Doi, M. Teranaka, H. Takashima, F. Goda, T. Idehara, I. Ogawa, and T. Idehara, Int. J. Infrared Millim. Waves **21**, 1155 (2000)
12. Tatsukawa *et al.*, Conf. Digest of 31th IRMMW & 14th THz (2006) p.577.
13. M. K. Hornstein, B. S. Bajai, R. G. Griffin, and R. J. Temkin, IEEE Trans. Plasma Sci. **34**, 524 (2006)
14. T. Idehara, I. Ogawa, La Agusu, T. Kanemaki, S. Mitsudo, T. Saito, *et al.* Int. J. Infrared Millim. Waves **28**(6), 433 (2007)
15. La Agusu, T. Idehara, H. Mori, T. Saito, I. Ogawa, and S. Mitsudo Int. J. Infrared Millim. Waves **28**(5), 315 (2007)

16. V. E. Zapevalov, V. K. Lygin, O. V. Malygin *et al.*, Conf. Digest of 29th IRMMW & 12th THz (2004) p.149.
17. T. Saito, T. Idehara, S. Mitsudo *et al.*, Conf. Digest of 31th IRMMW & 14th THz (2006) p.24.
18. N. I. Zaytsev, T. P. Panktratova, M. I. Petelin, and V. A. Flyagin, Radio Eng. Electron. Phys. **19**, 103 (1974)
19. T. Saito, T. Nakano, K. Sakai, *et al.*, Conf. Digest of Eighth IEEE International Vacuum Electronics Conference, pp. 345–346
20. T, Saito, T. Nakano, S. Mitsudo, I. Ogawa, and T. Idehara, Plasma and Fusion Research **2**, 024 (2007)
21. M. V. Kartikeyan, E. Borie, and M. K. A. Thumn, *Gyrotrons* (Springer, Berlin, 2004).
22. D. R. Whaley, M. Q. Tran, S. Alberti, T. M. Tran, T. M. Antonsen, and C. Tran, Phys. Rev. Lett. **75**, 1304 (1995)
23. M. Yeddulla, G. S. Nusinovich, and T. M. Antonsen, Phys. Plasmas **10**, 4513 (2003)
24. K. E. Kreischer and R. J. Temkin, Phys. Rev. Lett. **59**, 547 (1987)
25. M. V. Kartikeyan, E. Borie, and M. K. A. Thumn, IEEE Trans. Plasma Sci. **28**, 645 (2000)
26. G. S. Nusinovich, *Introduction to the Physics of Gyrotrons* (The Johns Hopkins University Press, Boltimore, 2004).
27. K. E. Kreischer, R. J. Temkin, H. R. Fetterman, and W. J. Mulligan, IEEE Trans. Microwave Theor. Tech. **MT-32**, 481 (1984)
28. S. Sabchevski, T. Saito, T. Idehara *et al.*, Submitted to Int. J. Infrared Millim. Waves (In press)